Structure of the hydrogen-stabilized MgO(111)-(1×1) polar surface: Integrated experimental and theoretical studies

V. K. Lazarov,[1] R. Plass,[1,*] H-C. Poon,[1] D. K. Saldin,[1] M. Weinert,[1] S. A. Chambers,[2] and M. Gajdardziska-Josifovska[1,†]
[1]*Department of Physics and Laboratory for Surface Studies, University of Wisconsin Milwaukee, P. O. Box 413, Milwaukee, Wisconsin 53201, USA*
[2]*Fundamental Science Directorate, Pacific Northwest National Laboratory, P. O. Box 999, Richland, Washington 99352, USA*
(Received 20 July 2004; revised manuscript received 19 October 2004; published 31 March 2005)

The surface structure of MgO(111)-(1×1) bulk and thinned single crystals have been investigated by transmission and reflection high-energy electron diffraction, low-energy electron diffraction (LEED), and x-ray photoelectron and Auger electron diffraction. The (1×1) polar surface periodicity is observed both after 800 °C annealing in air and also after oxygen plasma cleaning and annealing in ultrahigh vacuum. The x-ray photoelectron spectroscopy and diffraction results were analyzed by simulations based on path-reversed LEED theory and by first-principles calculations to help distinguish between different mechanisms for the stabilization of this extremely polar oxide surface: (1) stabilization by adsorption of a hydrogen monolayer; maintaining the insulating nature of the surface and (2) stabilization of the clean O or Mg terminated 1×1 surface by interlayer relaxations and two-dimensional surface metallization. The analysis favors stabilization by a single OH layer, where hydrogen sits on top of the O ions with O-H bond distance of 0.98Å. The in-plane O and Mg positions fit regular rocksalt sites, the distance between the topmost O and Mg plane is 1.04 Å, contracted by ~14% with respect to bulk MgO distance of 1.21 Å, while the interlayer separation of the deeper layers is close to that of bulk, contracted by less than 1%. The presence of a monolayer of H associated with the terminal layer of oxygen reduces significantly the surface dipole and stabilizes the surface.

DOI: 10.1103/PhysRevB.71.115434 PACS number(s): 68.47.Gh, 61.14.Qp, 68.49.Uv, 73.20.At

I. INTRODUCTION

The stability of polar oxide surfaces has long been a problematic question, as discussed in books on oxide surfaces[1,2] and recent reviews of polar oxide surfaces.[3,4] In the standard model, bulk-terminated polar oxide surfaces have diverging (surface) energies because alternating layers of oppositely charged ions produce a diverging electric dipole moment perpendicular to the surface, giving rise to the so-called "polar surface instability" problem. The rocksalt structure is often the most stable form for highly ionic solids, and has been the prototype for experimental and theoretical studies of neutral and polar oxide surfaces. The structure consists of two interpenetrating fcc lattices of oxygen anions and metal cations in a +2 oxidation state, making these oxides even more ionic than the prototypical ionic NaCl. The polar MgO(111) surface, consisting of equidistant alternating layers of oxygen and magnesium, in particular, has been an important test case of the polar instability problem.

In the 1970's, the polar oxide surface problem was considered settled, with a consensus between theory[5] and experiment[6,7] that clean MgO(111) polar surfaces do not exist, but facet into neutral {100} planes, and thereby making the surface energy finite. The first scanning electron microscopy (SEM) and low-energy electron diffraction (LEED) study of MgO(111) surfaces reported thermal faceting into three-sided pyramids.[6] The faces of these micropyramids were interpreted as the neutral {100} surfaces suggested by theory, although there were no direct measurements of the actual facet angles due to charging effects in LEED and the inability to quantify topography from single SEM images. Discovery of reconstruction-stabilized MgO(111) polar oxide surfaces by reflection high-energy electron diffraction (RHEED) and reflection electron microscopy (REM)[8,9] necessitated a revisiting of the faceting model. Plass *et al.*[10] showed that acid etching, rather than thermal annealing, is responsible for the reported faceting of the MgO (111) into three sided pyramids. Atomic force microscopy (AFM) and tomographic SEM measurement found the facets to be close to the higher index {332} planes instead of the neutral {100} planes.[4,10] Faceting as a stabilization mechanism requires mass transport that one would expect to happen at higher annealing temperatures. However, instead of inducing or promoting faceting, increasingly higher temperature annealing was found to have no effect on the faceting at low to moderate temperatures, and to erase the faceting at high temperatures, replacing it with reconstruction-stabilized flat (111) terraces with air stable reconstructions. The structure of the MgO(111)$(\sqrt{3}\times\sqrt{3})R30°$, (2×2), and $(2\sqrt{3}\times 2\sqrt{3})R30°$ reconstructions were studied by direct methods applied to transmission electron diffraction to find terminations given by periodic arrangements of oxygen trimers and single oxygen atoms.[11] The (2×2) reconstruction, also reported for NiO(111) (Refs. 12–14) and FeO(111),[15] fits well with the simple electrostatic prediction as the most favorable solution for (111) rocksalt oxide surfaces. The idea of an octopole as the smallest neutral building block of the rocksalt structure is the basis of these models.[16–18] The simple electrostatic octopolar model has been questioned by recent grazing x-ray diffraction experiments and first-principle calculations for the model MgO(111)-(2×2) surface, finding marked dependence of the (2×2) structure on thermodynamic parameters such as oxygen partial pressure and temperature. For example, Mg-covered terminations with peculiar insulating

electronic structure were favored in O-poor conditions, and the O-terminated octopole was favored in O-rich environments. Similarly, the remaining two reconstructions $(\sqrt{3}\times\sqrt{3})R30°$ and $(2\sqrt{3}\times 2\sqrt{3})R30°$ cannot be explained by the electrostatic models; recent work[19] suggests that the MgO(111)$(\sqrt{3}\times\sqrt{3})$ surface may have vacancies in the top Mg layer.

Within the ionic picture, the existence of a bulk terminated MgO(111)(1×1) surface is not allowed,[16,17] although this surface might be stabilized by the adsorption of foreign species. For example, hydrogen adsorption on an oxygen-terminated MgO(111) surface would satisfy the "sigma-half" criterion[3] (as would OH absorption on Mg terminated surface), and the huge electric fields/dipoles across the specimen would be canceled.[20]

As was discussed above, experimental data rule out faceting as a stabilization mechanism, and air-stable reconstructions at temperatures higher than 1200 °C stabilize the MgO(111) surface. However, the structure of MgO(111) at lower temperature (<950 °C) is still an open question. First-principles calculations[21,22] suggest a metallic character for MgO(111), and both quantum-mechanical calculations and classical (electrostatic) theory predict hydroxylation as a mechanism that will cancel polarity. Refson *et al.*[20] argue that the surface energy of hydroxylated MgO(111) would be smaller than MgO(100), the most stable surface in MgO. In this paper we report the experimental observation of the MgO(111)-(1×1) structure on bulk and thinned single crystals, and analyze the data to distinguish between the proposed stabilization models.

II. EXPERIMENTAL AND THEORETICAL METHODS

A. *Ex situ* experiments

Disks cut from single-crystal MgO(111) slabs were mechanically polished and dimpled, then etched to perforation in hot concentrated nitric acid, washed with water, sputtered with 5 keV Ar ions, and furnace annealed in air to 800 °C. The samples were transported through air to a Hitachi H9000-NAR high-resolution transmission electron microscope where the electron transparent regions were investigated by bright field imaging (BF-TEM) and by transmission high-energy electron diffraction (THEED). Similar preparations, but higher temperature anneals in vacuum and in air were used in our prior studies that resulted in reconstruction stabilized MgO(111) surfaces.[8–11,13]

B. *In situ* experiments

Two MgO single crystal slabs cut along the (111) plane were mechanically polished and cleaned with acetone and methanol solvents. One crystal was etched in hot concentrated nitric acid, washed with water, and furnace annealed in air to 800 °C. The second crystal was kept in the as-polished state. Once in ultrahigh vacuum, both crystals were further cleaned with oxygen plasma at room temperature, followed by annealing at 800 °C in UHV by electron beam bombardment on the back side of the Mo plate on which the MgO crystals were mounted. The structure of the top surface was studied by reflection high-energy electron diffraction (RHEED), low-energy electron diffraction (LEED), and by x-ray photoelectron and Auger electron diffraction (XPD). A Gammadata/Scienta SES 200 photoelectron spectrometer (XPS) with monochromatic Al $K\alpha$ x-ray source was used to study the chemical composition of the MgO(111) surface, and a computerized two-axis sample goniometer was employed to record the polar and azimuthal variations on the O 1*s* and Mg KLL emission intensities. A flood gun was used to minimize the effects of surface charging. Details about the experimental system can be found elsewhere.[23]

The preparations used for the MgO(111) surface in this work were also used in our recent studies of polar oxide interfaces formed by epitaxial growth of Fe_3O_4 film in a polar (111) orientation.[24] Such preparations have been used extensively in the same system for preparation of clean neutral MgO(100) surfaces without any detectable surface hydroxides.[25] The oxygen pressure in the chamber during plasma cleaning was $\sim 2\times10^{-5}$ Torr, as measured with an ion gauge not directly in the activated oxygen beam. Room-temperature exposure to activated oxygen for tens of minutes results in the removal of adventitious carbon, as judged by XPS. The only surface contamination present (other than H) was a trace of F. The amount of F on the surface was about 0.15–0.2 ML, compared to ~1 ML of OH. Sputtering was not used to avoid further damage to the polar surface. Subsequent annealing in high vacuum restored the crystallographic order in the surface lost during the mechanical polishing, as judged by significant improvements in the appearance of the LEED and RHEED patterns.

C. Theoretical analysis

Three different theoretical approaches have been used to analyze the x-ray photoelectron and Auger electron diffraction data: single and multiple scattering XPD in cluster geometry[26] and multiple scattering XPD in a slab geometry.[27] The results presented in this paper were obtained using the path-reversed photoelectron diffraction algorithm[28,29] based on the reciprocity theorem in a slab geometry. In this approach the wave amplitudes at different emitters can be found by propagating the electron backward from the detector to the emitter. The photoelectron intensity is then evaluated by multiplying these amplitudes by the atomic photoelectron matrix elements. In Auger electron diffraction, the matrix elements are replaced by atomic Auger matrix elements. Since the latter are not as easy to evaluate numerically, we have assumed isotropic emitters for simplicity. This approximation is not expected to cause significant errors in the range of electron energies considered.

The MgO(111) crystal was divided into layers consisting either of Mg or O atoms with alternating stacking. The terminating layer was varied to be Mg, O, and OH, as proposed previously. Variations that move the topmost H and O layers to nonstandard lattice sites were also explored, as were double and triple OH layers. The layer diffraction matrices were found using a conventional LEED package.[30] Propagation of the electron from the detector to the emitter, with multiple scattering among different layers, was performed by

the renormalized forward scattering (RFS) algorithm.[30,31] Both the atomic matrix elements and phase shifts were calculated from a potential constructed using the program MUFPOT.[31]

R factor analysis was initially performed for interlayer spacing optimization for atomic models with and without hydrogen. The weak scattering of the oxygen photoelectrons and magnesium Auger electrons by hydrogen ions produces subtle differences between the calculated model XPD patterns, reducing the sensitivity of model refinements. To overcome this limitation, first-principles density functional theory (DFT) calculations were used to calculate optimized atomic positions for each model. Then the path-reversed algorithm was used to calculate XPD patterns for these positions, and an *R* factor analysis was performed to compare with the experimental XPD data, without further structural optimizations.

The DFT equations were solved using the full-potential linearized augmented plane wave (FLAPW) method[32,33] as implemented in the FLAIR code. Ground-state atomic geometries for all surface terminations were obtained by minimizing the forces and total energies. The calculated MgO bulk lattice constants for both the local density approximation (LDA) value of 4.194 Å and the generalized gradient approximation (GGA) value of 4.266 Å are in good agreement with the experimental MgO bulk lattice constant of 4.217 Å; we choose to use LDA in this study because of the slightly better agreement with experiment.

The surfaces were modeled by repeated slabs of between 13 and 39 layers. Calculations of polar surfaces in a slab geometry required particular care due to the long-range Coulomb interactions. One way to avoid this problem is to construct slabs that are symmetrically terminated [i.e., with odd numbers of close packed (111) layers]. We have tested that our reported results are essentially unchanged with respect to increasing the number of layers, the "vacuum" region, the Brillouin zone sampling, and the basis size cutoffs. The relatively large number of layers [compared to four or five layers used in prior MgO(111) calculations] was selected to reproduce the bulk interplanar distances in the middle of the slab, to give better quantitatively reliable calculated surface interplanar spacings, as well as allowing for a clearer separation between surface and bulk contributions.

III. EXPERIMENTAL RESULTS

A. *Ex situ* THEED experiments

Figure 1(a) shows a selected area THEED pattern with pronounced (1×1) spots. The bright field TEM images from the same area [Fig. 1(b)] reveal terrace and step structures. The terraces must have (111) character to allow the observation of the surface specific (111)-1×1 spots [indicated with arrows in Fig. 1(a)], which are forbidden for bulk MgO, having fractional Muller indices of $\frac{1}{3}(422)$ type. These $(111)1\times1$ reflections are not commonly observed in electron diffraction data from MgO powder or bulk samples that tend to be terminated by neutral (100) type surfaces. To the best of our knowledge this is the first observation of rocksalt

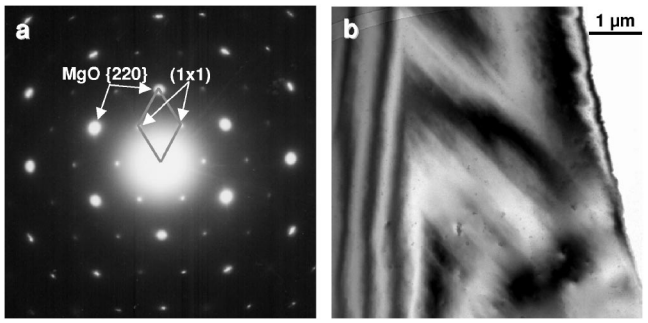

FIG. 1. THEED (a) and bright field TEM (b) of an electron transparent MgO(111) sample annealed at 800 °C in air. Reflections marked by arrows in (a) denote a 1×1 surface structure.

(111)-1×1 THEED patterns. We have observed these reflections, along with additional reconstruction specific reflections, in our earlier THEED patterns from MgO(111) surfaces with $(\sqrt{3}\times\sqrt{3})R30°$, (2×2) and $(2\sqrt{3}\times2\sqrt{3})R30°$ structures obtained at much higher annealing temperatures.[11]

The forbidden $\frac{1}{3}(422)$ reflections were first reported in THEED patterns from Au foils terminated with (111)-1×1 surfaces and identified as surface truncation spots.[34] These bulk forbidden reflections remain extinguished when the specimen has a complete number of bulk unit cells in the propagation direction of the incident beam [i.e., thickness $=3N$, where N is the number of close packed (111) Au plane], but become visible for incomplete number of bulk unit cells (i.e., sample thickness of $3N\pm1$ atomic layers). The same analysis and conclusions can be applied to our observation of the MgO(111)-1×1 reflections, but N here becomes the number of Mg-O(111) bilayers.

We have previously used the surface reconstruction spot intensity from THEED to propose structures for the reconstructed MgO(111) surfaces,[11] but the 1×1 reflections were omitted from these analyses because they contain contributions from incomplete numbers of unit cells in the electron beam direction. THEED is a powerful method for finding in-plane positions, but not for out-of-plane relaxations.[35] For this reason we undertook further diffraction and spectroscopy experiments to gain information about the MgO(111)-1×1 surface structure and composition under controlled vacuum conditions.

B. *In situ* LEED and RHEED experiments

Upon oxygen plasma cleaning and annealing in UHV, both MgO(111) single crystal samples displayed (1×1) LEED (Fig. 2) and RHEED (Fig. 3) patterns, in agreement with the THEED observations after air anneals. RHEED from the acid-etched and annealed crystals displayed some transmission contributions, as expected from our previous observations of vicinal faceting of MgO surfaces upon acid etching.[10,36] The LEED patterns shown in Fig. 2 are from a polished, plasma-cleaned, and UHV-annealed crystal. These LEED patterns show a 1×1 surface structure without threefold splitting which had been observed previously on faceted MgO(111) surfaces.[6] At present we do not have experimental LEED *I-V* curves from these surfaces. Instead, we use angle-

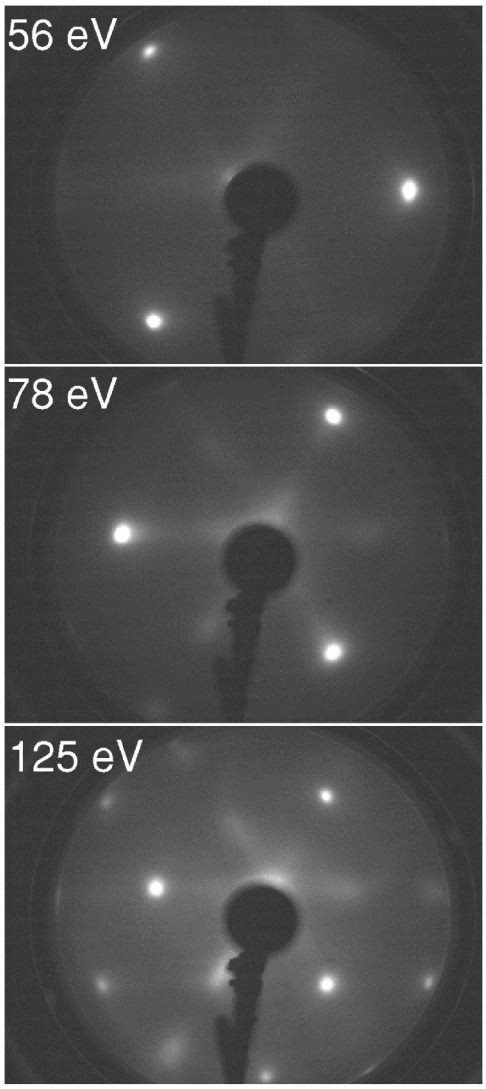

FIG. 2. LEED patterns for the MgO(111)-1×1 surface obtained by oxygen plasma cleaning and annealing at 800 °C in UHV. A 1×1 surface periodicity is evident at all three energies.

resolved x-ray photoelectron core-level spectroscopy, and scanned angle x-ray photoelectron and Auger electron diffraction (XPD/AED) to probe the MgO(111)-(1×1) surface composition and structure.

C. *In situ* XPS/XPD experiments

Scanned-angle XPD/AED at low take-off angles enhances the surface sensitivity of the technique. We have thus measured O 1*s* and Mg *KLL* azimuthal angular distributions at take-off angles ranging from 7° to 16°, as well as polar scans in high-symmetry azimuths [Fig. 4(a)]. The (1×1) surface termination is readily determined from qualitative considerations of the polar scans, at least for this particular crystal type and surface orientation. The O 1*s*/Mg *KLL* intensity ratio is expected to increase (decrease) as grazing emission is approached if the surface is terminated with O (Mg), due simply to inelastic attenuation of outgoing photoelectrons. We have found that this ratio increases at low take-off angles

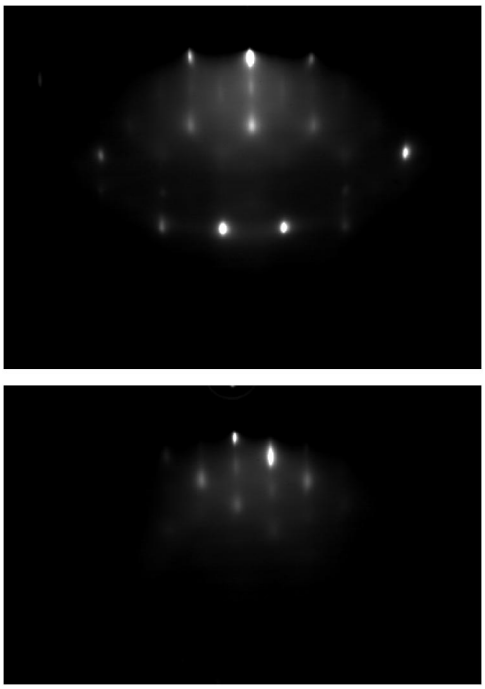

FIG. 3. RHEED patterns of MgO(111)-(1×1) surface as prepared in Fig. 2. The upper and lower panels show the patterns along the [11-2] and [1-10] azimuths, respectively.

in all low-symmetry azimuths, as seen in Fig. 4(b) for polar angles smaller than 15°, favoring the O and OH termination models over the Mg termination model. A detailed theoretical analysis of the XPD data is presented in Sec. IV, which favors the OH termination.

High-energy-resolution O 1*s* spectra obtained at normal emission ($\theta=90°$) and grazing emission ($\theta=10°$) reveal a surface specific peak that is shifted by ~2 eV towards higher binding energy, as shown in Fig. 5. This peak can be ascribed to the presence of a terminal layer of OH based on the nearly identical chemical shift measured for dissociative chemisorption of water on MgO(001).[37] However, the observed O 1*s* shift on the polar surface cannot be used to unambiguously exclude the O-terminated model without independent knowledge of the magnitude and shift direction that would be produced by the predicted two-dimensional (2D) metallization and interlayer relaxation. The DFT calculations of the O 1*s* and 2*s* levels discussed in Sec. IV confirm the OH termination interpretation, allowing us to label the shifted peak in Fig. 5 as an OH peak. The angular dependence of the OH peak intensity, relative to that of lattice oxygen, shows that the amount of OH is equal to ~1 ML if the O 1*s* photoelectron escape length is assumed to be 30–35 Å, which is not unreasonable for a wide band gap insulator such as MgO.

IV. THEORETICAL ANALYSIS

A. Atomic structure from DFT and XPD/AED

Several structural models were constructed for the MgO(111)-(1×1) surface, as summarized in Table I. For all models, the in-plane and out-of-plane atomic positions were

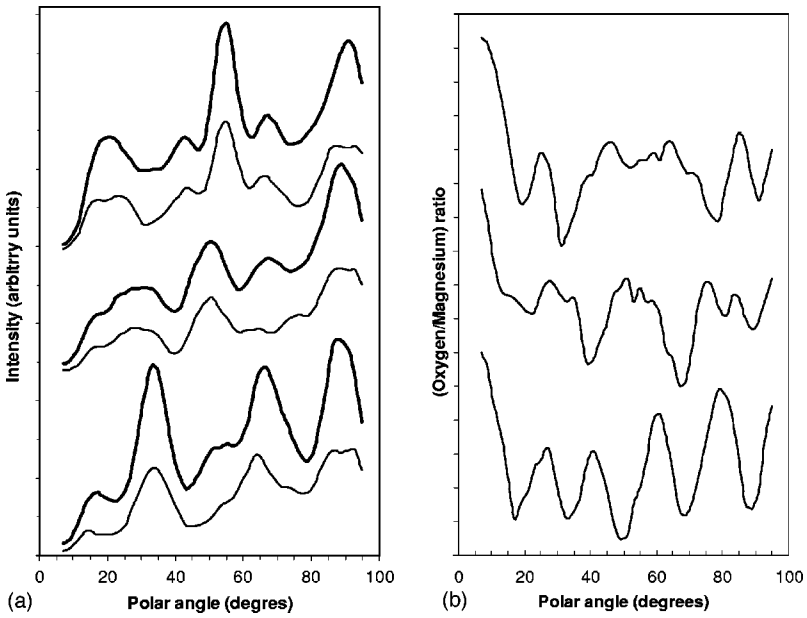

FIG. 4. (a) XPD polar scans in three high symmetry azimuths (ϕ=0°, 30°, and 60°) showing the Mg *KLL* Auger (bold line) and the O 1*s* photoelectron (thin line) integrated intensity as function of take off angle. (b) O 1*s*/Mg *KLL* intensity ratio vs polar angle for same azimuths. This ratio increases at low take-off angles (i.e., polar angles smaller than 15°) indicating that the terminating layer is oxygen rich.

optimized by minimization of the atomic forces in the DFT total energy calculations. In Table I we report only the first three important interplanar distances between the O and Mg close-packed (111) planes: d_1 is the distance between the two topmost planes (e.g., between the first O and the second Mg plane for O-terminated and OH-terminated surfaces, or between the first Mg and second O plane for the Mg-terminated surface), d_2 is the distance between the second and third planes, and d_3 between the third and fourth planes.

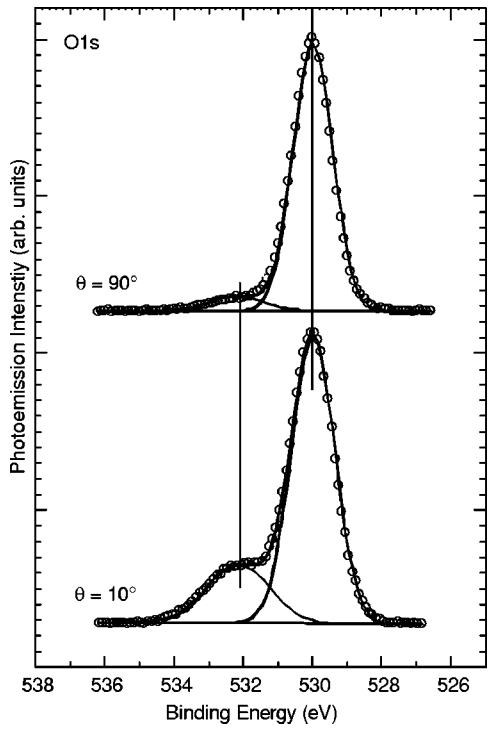

FIG. 5. XPS of O 1*s* peak for normal (θ=90°) and grazing take-off angles showing surface specific shift toward higher binding energy indicative of OH termination of the UHV annealed MgO(111) surface.

The first two models are for clean Mg- and O-terminated surfaces. The interlayer separations for the Mg-terminated surface are close to the bulk value, the first layer is expanded by 3.6%, while the second and third layer are contracted by 0.3 and 0.2 %, respectively. In contrast, the clean O-terminated surface layer contracts by 29.4% from the bulk value, the second Mg layer expands by 9.4%, and the third O layer is contracted by 6.3%.

The H-terminated model, with an H on top of every O and the O in regular rocksalt stacking sites, has an H-O distance of 0.98 Å. Total energy calculations favor H on top of O instead of the hollow site by 0.16 eV. The OH bond length is expanded by 7.2% with respect to the bulk OH distance in $Mg(OH)_2$. The first O-Mg distance of 1.041 Å is expanded by 8.6% from the corresponding bulk $Mg(OH)_2$ distance of 0.958 Å, and contracted by 14.4% from the bulk MgO distance of 1.217 Å. The second and third interlayer distances are close to the bulk oxide value, displaying contractions of 0.8 and 0.5 %.

The next three models with two OH groups cover the options of having H between the second and third layer in addition to its presence as a top layer. Three models were considered: (i) H on top of the first O layer and H beneath the O of the second layer, (ii) H on top of the first O layer and H in a hollow site between the second and third layers, and (iii) H on top of the first O layer and half a monolayer of H beneath the second O layer. For all three cases, the topmost H (as in the case with a single OH model) induced a contraction for the first (O-Mg) interlayer distance in the 11–14 % range. The second Mg-O interplanar distance is contracted by 2.1% in case (i), but expanded by 3.1 and 18.1 % for cases (ii) and (iii). Finally the third O-Mg interplanar distance was expanded in all three cases, by 51.6, 72.9, and 59.4 % with respect to bulk MgO interplanar distances, respectively. It is not unexpected that the presence of an H plane between the second and third layer should yield significantly enlarged the O-Mg distance.

The last model considered has three OH layers whose structure is based on the $Mg(OH)_2$ (brucite) structure. The

TABLE I. The topmost Mg-O or O-O distances used for XPD calculation. Pendry's R factor (R_P) averaged over Mg KLL and O 1*s* spectra for electron intensities as a function of polar angles along the [110] are presented.

Model	d_1(Å)	d_2(Å)	d_3(Å)	R_P(Å)
Mg/O/Mg Mg terminated	1.254	1.207	1.208	0.24
O/Mg/O O-terminated	0.855	1.325	1.135	0.21
H/O/Mg/··· OH terminated	1.041	1.206	1.209	0.19
H/O/Mg/··· OH terminated with stacking fault	1.067	1.276	1.215	0.26
H/O/Mg/O/H/Mg/O OH on top with a monolayer of H in second O plane	1.050	1.185	1.836	0.35
H/O/Mg/O/H/Mg/O OH on top with a monolayer of H in hollow beneath second O plane	1.078	1.248	2.093	0.37
H/O/Mg/O/H/Mg/O OH on top with a halve monolayer of H in second O plane	1.047	1.429	1.929	0.44
H/O/Mg/O/H/H/O Brucite with OH on top	1.118	1.245	2.795	0.41

first O-Mg plane distance in brucitelike termination of MgO(111) had a contraction of 2.5%, while the second Mg-O planar distance is expanded by 2.8%. The third interplanar O-Mg distance in brucitelike models is distinct from the previous models, due to the missing Mg plane being replaced by the double H layers. Thus the third planar distance was determined to be 130.9% larger than bulk MgO.

The three topmost planar DFT optimized distances, excluding the H planes because of their negligible scattering power, were used for XPD calculations. A quantitative comparison between the theoretical and the experimental XPD results is provided by Pendry's R factor R_P.[38] The R factor analysis, given in Table I, shows that the best fit to the experimental data is given by the OH-terminated surface, with a single monolayer of H on top of an oxygen layer in a regular rocksalt lattice site. However, the difference in R factors is rather small, especially between the O-terminated and the single OH-terminated models, necessitating further analysis of the XPD line shapes.

Figure 6 shows the calculated Mg *KLL* Auger electron diffraction intensities and the calculated O 1*s* photoelectron diffraction intensities as a function of polar angle along azimuth [110], for the clean Mg- and O-terminated surfaces and for the OH-terminated structural models obtained from the total energy calculations. Since hydrogen atoms have negligible cross section in the medium energy range, the H-terminated and O-terminated surfaces have the same stacking sequence and differ only in their surface relaxations as obtained by the total energy calculation. The experimental data are also shown. The prominent peaks at 54.7° (with respect to surface normal) are due to both the focusing[39,40] and defocusing[41] effects along an internuclear axis joining the atoms in adjacent atomic layers. Therefore, this azimuth is expected to have the greatest sensitivity to the surface structure.

In Fig. 7 we compare the azimuthal dependence of the calculated ratio of the Mg *KLL* to O 1*s* intensities and the corresponding experimental data for electrons exiting at a glancing angle of 7° with respect to the surface. If we ignore the difference in scattering factors of the two atomic species and the relatively small difference in electron energy, both the Auger and photoelectron emitters have the same structural environment in the bulk. Taking the ratio would enhance the difference that is mainly due to the structure near

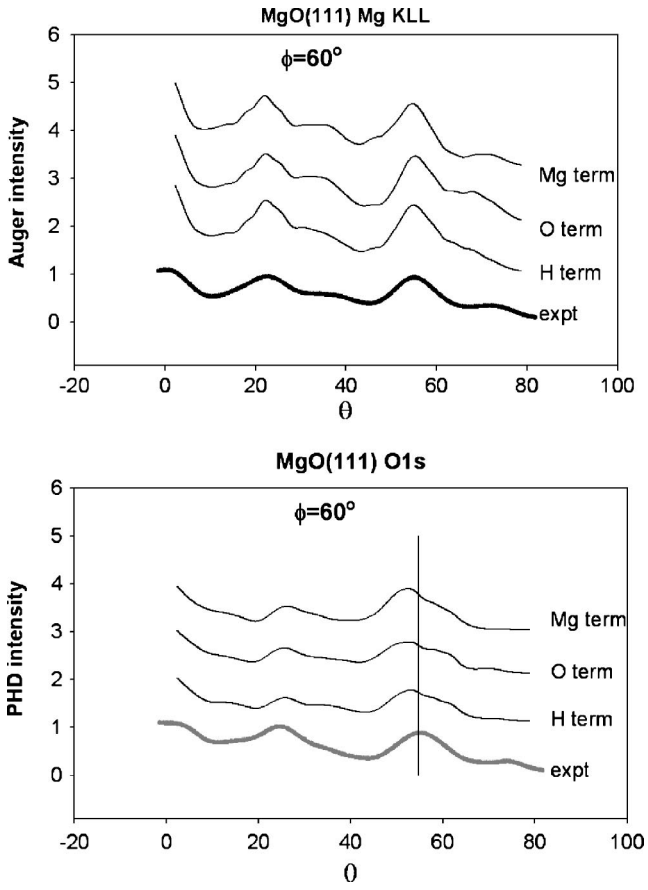

FIG. 6. Calculated Mg *KLL* Auger intensities and O 1*s* photoelectron intensities as function of polar angle (measured from surface plane) along the [110] azimuth, assuming Mg-, O-, and OH-terminated MgO(111)-(1×1) structural models with distances obtained from the total energy calculations. The corresponding experimental results are shown as bold lines.

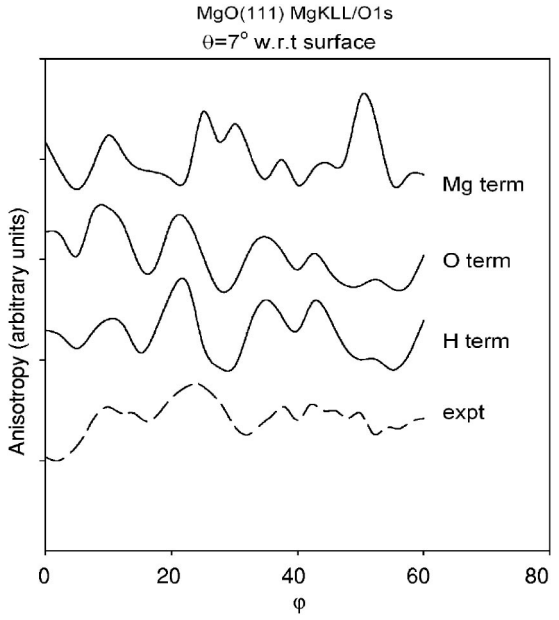

FIG. 7. Calculated azimuthal Mg *KLL*/O 1*s* intensity ratios for the models shown in Fig. 6, and the corresponding experimental data for electrons exiting at a glancing angle of 7° with respect to the surface. The best fit is obtained for the OH-terminated surface structure.

the surface. The different models do show considerable sensitivity to the surface structure. As seen from the figure, the Mg-terminated model can be excluded. For the OH- and O-terminated models, the relative intensities of peaks favor the former model. We also note that there are shifts between the calculated and experiment peaks which could be due to uncertainty in sample alignment.

B. Electronic structure from DFT calculations

In addition to structural properties, the FLAPW calculations provide information about the electronic properties of the systems. The local density of states (LDOS), shown in Fig. 8, show the valence band and the deep-lying O 2*s* states, and provide unique signatures for the preferred surface termination. Figures 8(a)–8(c) shows the LDOS of the top Mg and O layers for the Mg, O, and OH terminations. The bulk LDOS for the Mg and O are also presented for reference in Fig. 8(d). For both O and Mg termination, the top layers have states around the Fermi level, indicative of the proposed 2D metallic character of both surfaces. The DOS of the top O layer are derived from the O valence band, while in the Mg terminations the states around the Fermi energy in the middle of the gap are derived mainly from the conduction Mg band. In contrast, the OH-terminated surface does not exhibit metallic (partially occupied) states, but the surface band gap is reduced by 70% with respect to bulk MgO because of the H-induced surface states in the gap. Experimental recording of valence band photoelectron spectra is precluded by the long counting times (several hours) during which charging causes slow drifts in the binding energy scale that are hard to compensate by flood guns. UPS was further

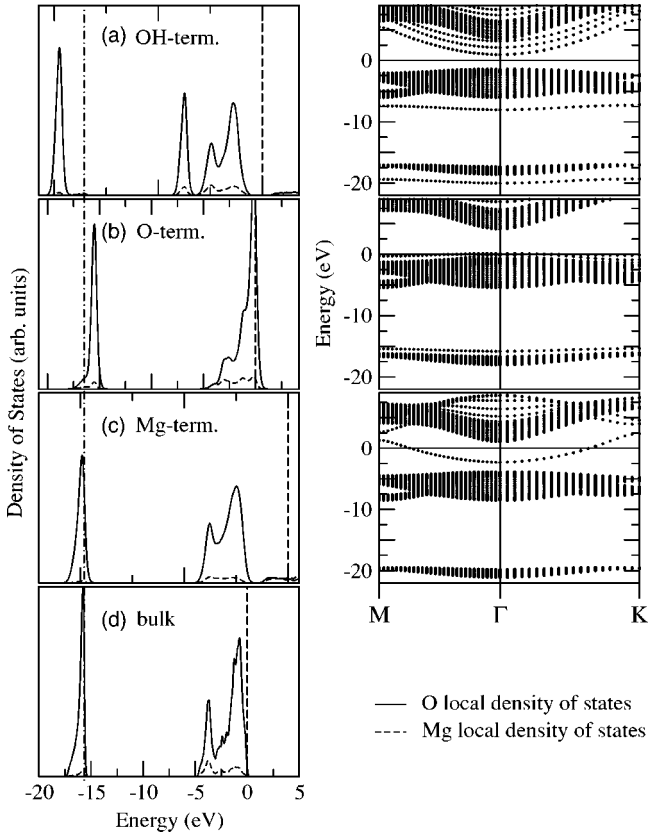

FIG. 8. Local density of states for the topmost O and Mg atomic planes for slabs terminated with (a) OH, (b) O, and (c) Mg, and (d) for bulk MgO. The dashed vertical lines represent the Fermi levels, showing the insulating nature of the OH termination, and the metallic nature of the O and Mg terminations. (The "bulk" atoms of the different calculations are used to align the energies.) Comparison with the position of bulk O 2*s* level (dashed-dotted line) shows a shift to higher (lower) binding energy for OH (O) termination. The band structure for the three terminations is shown on the right for the OH (top), O (middle), and Mg (bottom) terminations.

complicated by charging because the He source is so much brighter than the x-ray source.

For the OH termination, the O-derived 2*s* states at the surface display a ~2 eV shift towards higher binding energy [Fig. 8(a)], and the 1*s* states are shifted by ~1 eV (not shown). These shifts are in the same direction as the experimental shift of 2 eV seen in the XPS spectra in Fig. 5. For the O termination, the calculations a −1 eV shift of the 2*s* surface state and −0.2 eV of the 1*s* state, both towards lower binding energy and in the *opposite* direction from the experiment. The shifts of the O 1*s* and 2*s* states for the Mg-terminated slabs are essentially zero, in contrast to the experimentally observed shifts. These trends can also be seen in the dispersion of the surface and bulk bands for the three models, as shown to the right in Fig. 8. The different terminations also will affect the surface dipole, and hence the work functions of the system. The H changes the density significantly in the surface region, and thereby reducing the surface dipole of the O-terminated surface by several eV, leading to a work function for the OH-terminated surface of ~3.6 eV.

The above calculations also allow for spin polarization. While the oxygen-terminated surface has a calculated magnetic moment, this moment is quenched when hydrogen is adsorbed. The changes in the calculated structural properties for the magnetic O-terminated surface are small compared to the scale needed for noticeable differences in the *R* factor. Regarding the possibly more significant changes in the electronic properties with surface magnetism, especially with regard to the shifts in the density of states, the basic physics and conclusions are the same as for a nonmagnetic surface: For the magnetic O-terminated surface, the (fully occupied) majority DOS were found to be aligned with the bulk O DOS, while the minority DOS are again shifted towards lower binding energy (with the shift large for magnetic O), opposite to the shift for OH termination.

V. DISCUSSION AND CONCLUSIONS

Our experimental and theoretical results favor the OH-terminated model over the stoichiometric O-terminated or Mg-terminated models for this polar oxide surface, in agreement with prior theoretical predictions of dipole moment and surface energy minimization provided by the OH termination.[19,42,43] The interlayer separations obtained in our DFT calculations and XPD experiments are in close agreement with recently published DFT results for this surface.[43] In addition, we have considered new models with double and triple OH layers in a $Mg(OH)_2$ configuration. These models generate poorer fits to the experimental data; however, they could be used in modeling of the initial steps of bulk hydroxylation studied recently by environmental electron microscopy.[44]

Hydrogen is difficult to detect in electron diffraction experiments due to its small scattering factor. Our XPD results indicate that the OH termination with the first O-Mg contraction of 14.4% presents only a slightly better fit to the experiments than the O termination with contraction of 29.4%. However, it is important to note that our DFT calculations indicate that the O core levels can be used to easily discriminate between the O and the OH termination, because they give chemical shifts in opposite directions.

Our results pointing to H stabilization of the MgO(111) surface suggests that an unreconstructed stoichiometric (111) surface remains as yet unobserved. It is notable that the hydrogen termination is present even upon oxygen plasma cleaning of the native MgO(111) surface followed by 800 °C annealing under ultrahigh vacuum ($\sim 10^{-11}$ Torr). The same preparation conditions have been found to yield hydrogen-free neutral MgO(100)-(1×1) surfaces. The source of the surface hydrogen in the MgO(111) experiments is not fully understood. It could be present on the native (111) surface via interaction with atmospheric water, as suggested by the theoretical study of Refson *et al.*[20] that showed the hydroxylated MgO(111) face to be more stable than the (100) orientation. These authors have argued that the interaction with water drives the frequent occurrence of (111) terminations on geological MgO (periclase) samples. Once formed, the OH termination would provide a very effective stabilization of the polar surface and might be present at the native surfaces, as also suggested for $\alpha-Al_2O_3(0001)$.[45] Indeed, our recent follow up XPS experiments with air exposed unreconstructed MgO(111) surfaces found a strong OH signal that is reduced upon annealing in UHV, but not eliminated.[46] At this time we cannot determine if this native hydroxide termination is impervious to the oxygen plasma cleaning and UHV annealing that were used in the present work, or if the hydrogen termination is removed and then reformed upon cooling by adsorption of atomic hydrogen or by dissociative chemisorption of H_2 or H_2O from the UHV ambient. These results suggest that polar oxide surfaces may be of interest for splitting water and/or hydrogen storage.

Apart from the effects of the annealing temperature and pressures, the crystal thickness in the polar direction also merits discussion. In our study we find the MgO(111)-(1×1)-OH structure on both macroscopic single crystals and on thinned unsupported single crystals of thickness ranging from few nanometers to several hundred micrometers. All prior reports of the (111)-(1×1)-OH surface structure have been for ultrathin films of NiO, CoO, and FeO grown on metal substrates, using spectroscopic methods to determine the presence of hydrogen, and diffraction methods to document the 1×1 periodicity.[3] To the best of our knowledge there are no reported surface structure determinations for the (111)-(1×1)-OH atomic positions in these thin films. A reversible (1×1)-OH to $p(2\times2)$ reconstruction has been reported for 1–2 nm thin films of NiO(111) on Ni(111) upon heating in UHV and readsorption of water.[47] However, the single crystal NiO(111)-(2×2) surfaces were not found to transform to a (1×1)-OH structure upon water exposure under conditions that readily transform the thin films.[14] In this sense our elucidation of the MgO(111)-(1×1)-OH surface structure marks a first such finding on a bulk rocksalt oxide crystal.

A few reports of unreconstructed surfaces exist for ultrathin oxide films grown in the polar direction on metal substrates. A 14.8% contraction of the O-Ni interplanar separation was reported for O-terminated NiO(111) films on Ni(100) substrates from LEED,[48] but hydrogen was not included in the models. This result has not been reproduced in other studies of NiO(111) films. A bulk-terminated 1×1 structure has also been reported for a single bilayer of FeO(111) on Pt(111),[49] and for a single trilayer of NaCl(111) on Al(111),[50] but such ultrathin polar surface structures on macroscopic metal substrates are expected to have different stabilization behavior. Most recently Kiguchi *et al.*[51] have shown that a rather flat unreconstructed polar MgO(111)-(1×1) could be grown by alternate adsorption of Mg and O_2 on Ag(111). While the absence of hydrogen has not been directly proven, electron energy loss spectroscopy (EELS) and ultraviolet photoelectron spectroscopy (UPS) results indicate that the surface is semiconducting or metallic, in contrast to the insulating nature expected for the OH termination.

In conclusion, our combined experimental and theoretical study shows that hydrogen stabilizes the MgO(111) polar oxide surface. In addition, we report on the structural determination of a (111)-(1×1)-OH surface for a polar rocksalt crystal.

ACKNOWLEDGMENTS

This study was sponsored by the National Science Foundation (Grant No. NSF/DMR-95531489), the Research Corporation (Grant No. RA0331), and the U.S. Department of Energy (Grant No. DE-FG02-84ER45076). The *in situ* experiments were performed in the Environmental Molecular Sciences Laboratory, a national scientific user facility sponsored by the Department of Energy's Office of Biological and Environmental Research located at Pacific Northwest National Laboratory. We would like to thank Mark Pauli for cluster XPD calculations in the early stages of this study.

*Current address: Sandia National Labs, M.S. 1310, P.O. Box 5800, Albuquerque, NM 87185, USA.

†Electronic address mgj@uwm.edu

[1] V. E. Henrich and P. A. Cox, *The Surface Science of Metal Oxides* (Cambridge University Press, Cambridge, 1994).

[2] C. Noguera, *Physics and Chemistry at Oxide Surfaces* (Cambridge University Press, Cambridge, 1996).

[3] C. Noguera, J. Phys.: Condens. Matter **12**, R367 (2000).

[4] M. Gajdardziska-Josifovska, R. Plass, M. A. Schofield, D. R. Giese, and R. Sharma, J. Electron Microsc. **51**, S13 (2002).

[5] P. W. Tasker. J. Phys. C **12**, 4977 (1979).

[6] V. E. Henrich, Surf. Sci. **57**, 385 (1976).

[7] H. Onishi, C. Egawa, T. Aruga, and Y. Iwasawa, Surf. Sci. **191**, 479 (1987).

[8] M. Gajdardziska-Josifovska, P. A. Crozier, and J. M. Cowley, Surf. Sci. Lett. **248** L259 (1991).

[9] P. A. Crozier, M. Gajdardziska-Josifovska, and J. M. Cowley, Microsc. Res. Tech. **20**, 426 (1992).

[10] R. Plass, J. Feller, and M. Gajdardziska-Josifovska, Surf. Sci. **414**, 26 (1998).

[11] R. Plass, K. Egan, C. Collazo-Davila, D. Grozea, E. Landree, L. D. Marks, and M. Gajdardziska-Josifovska, Phys. Rev. Lett. **81**, 4891 (1998).

[12] C. A. Ventrice, Jr., Th. Bertrams, H. Hannemann, A. Brodde, and H. Neddermeyer, Phys. Rev. B **49**, 5773 (1994).

[13] M. Schofield, Ph.D. thesis, University of Wisconsin, Milwaukee, 1999.

[14] A. Barbier, C. Mocuta, H. Kuhlenbeck, K. F. Peters, B. Richter, and G. Renaud, Phys. Rev. Lett. **84**, 2897 (2000).

[15] D. Cappus, M. Haßel, E. Neuhaus, M. Heber, F. Rohr, and H.-J. Freund, Surf. Sci. **337** 268 (1995).

[16] D. Wolf, Solid State Ionics **75**, 3 (1995).

[17] D. Wolf, Phys. Rev. Lett. **68**, 3315 (1992).

[18] F. Finocchi, A. Barbier, J. Jupille, and C. Noguera, Phys. Rev. Lett. **92**, 136101 (2004).

[19] A. Subramanian, L. D. Marks, O. Warschkow, and D. E. Ellis, Phys. Rev. Lett. **92**, 026101 (2004).

[20] K. Refson, R. A. Wogelius, D. G. Fraser, M. C. Payne, M. H. Lee, and V. Milman, Phys. Rev. B **52**, 10823 (1995).

[21] M. Tsukada and T. Hoshino, J. Phys. Soc. Jpn. **51**, 2562 (1982).

[22] J. Goniakowski and C. Noguera, Phys. Rev. B **60**, 16120 (1999).

[23] S. A. Chambers, Surf. Sci. Rep. **39**, 105 (2000).

[24] V. K. Lazarov, S. A. Chambers, and M. Gajdardziska-Josifovska, Phys. Rev. Lett. **90**, 216108 (2003).

[25] S. A. Chambers (unpublished).

[26] A. P. Kauwela, G. S. Herman, D. J. Friedman, and C. S. Fadley, Phys. Scr. **41**, 948 (1990); D. K. Saldin, G. R. Harp, and X. Chen, Phys. Rev. B **48**, 8234 (1993).

[27] C. H. Li, A. R. Lubinsky, and S. Y. Tong, Phys. Rev. B **17**, 3128 (1978).

[28] M. D. Pauli and D. K. Saldin, Phys. Rev. B **64**, 075411 (2002).

[29] H. C. Poon, M. D. Pauli, A. Wander, and D. K. Saldin, Phys. Rev. B **65**, 134115 (2002).

[30] M. A. Van Hove and S. Y. Tong, *Surface Crystallography by LEED* (Springer, Berlin, 1979).

[31] J. B. Pendry, *Low Energy Electron Diffraction* (Academic, London, 1974).

[32] E. Wimmer, H. Krakauer, M. Weinert, and A. J. Freeman, Phys. Rev. B **24**, 864 (1981).

[33] M. Weinert, E. Wimmer, and A. J. Freeman, Phys. Rev. B **26**, 4571 (1982).

[34] D. Cherns, Philos. Mag. **30**, 549 (1974).

[35] L. D. Marks, E. Bengu, C. Collazo-Davila, D. Grozea, E. Landree, C. Leslie, and W. Sinkler, Surf. Rev. Lett. **5**, 1087 (1998).

[36] D. R. Giese, F. J. Lamelas, H. A. Owen, R. Plass, and M. Gajdardziska-Josifovska, Surf. Sci. **457**, 326 (2000).

[37] P. Liu, T. Kendelewicz, G. E. Brown, Jr., and G. A. Parks, Surf. Sci. **412/413**, 287 (1998).

[38] J. B. Pendry, J. Phys. C **13**, 937 (1980).

[39] H. C. Poon and S. Y. Tong, Phys. Rev. B **30**, R6211 (1984).

[40] S. Mroz, M. Nowicki, and A. Krupski, Prog. Surf. Sci. **74**, 109 (2003).

[41] S. Y. Tong, H. C. Poon, and D. R. Snider, Phys. Rev. B **32**, 2096 (1985).

[42] A. Pojani, F. Finocchi, J. Goniakowski, and C. Noguera, Surf. Sci. **387**, 354 (1997).

[43] A. Wander, I. J. Bush, and N. M. Harrison, Phys. Rev. B **68**, 233405 (2003).

[44] M. Gajdardziska-Josifovska and R. Sharma, Microsc. Microanal. (to be published).

[45] S. A. Chambers, T. Droubay, D. R. Jennision, and T. R. Mattsson, Science **297**, 827 (2002)

[46] E. Lu, P. Lyman, V. K. Lazarov, and M. Gajdardziska-Josifovska (unpublished).

[47] F. Rohr, K. Wirth, J. Libuda, D. Cappus, M. Baumer, and H.-J. Freund, Surf. Sci. Lett. **315**, L977 (1994).

[48] O. L. Warren and P. A. Thiel, J. Chem. Phys. **100**, 659 (1994).

[49] M. Ritter, W. Ranke, and W. Weiss, Phys. Rev. B **57**, 7240 (1998).

[50] W. Hebenstreit, M. Schmid, J. Redinger, R. Podloucky, and P. Varga, Phys. Rev. Lett. **85**, 5376 (2000).

[51] M. Kiguchi, S. Entani, K. Saiki, T. Goto, and A. Koma, Phys. Rev. B **68**, 115402 (2003).